



## ACTIVE CONFINEMENT FOR STRENGTH AND DUCTILITY ENHANCEMENT OF CONCRETE USING Fe-SMA STRIPS

S.K. Deb<sup>(1)</sup>; M. Sarmah<sup>(2)</sup>; and A. Dutta<sup>(3)</sup>

<sup>(1)</sup> Professor, Civil Engineering Dept., IIT Guwahati, Assam 781039, India. E-mail: skdeb@iitg.ac.in

<sup>(2)</sup> Ph.D. Student, Civil Engineering Dept., IIT Guwahati, Assam 781039, India. E-mail: monjushasarmah@iitg.ac.in

<sup>(3)</sup> Professor, Civil Engineering Dept., IIT Guwahati, Assam 781039, India. E-mail: adutta@iitg.ac.in

### Abstract

Active confinement of concrete is superior to passive confinement in terms of increasing concrete strength and ductility under the same confinement pressure. This is because, in the case of passive confinement, concrete would have to undergo dilation in order to fully activate the confinement pressure. However, in the active confinement approach, there is a delay in damage sustained by concrete due to early application of the confinement pressure before concrete dilation.

Active confinement of concrete using Shape Memory Alloy (SMA) has demonstrated effectiveness in increasing its strength and ductility significantly. This technique utilizes the high recovery stress, developed during thermal activation of pre-strained SMA spirals/strips, to apply active confining pressure on concrete. A cost-effective iron-based SMA (Fe-SMA) with composition Fe-17Mn-5Si-10Cr-4Ni-1(V, C) has been developed at EMPA (Swiss Federal Laboratories for Materials Science and Technology) for pre-stressing applications in civil engineering structures. There are a few experimental studies on application of Fe-SMA in various civil engineering problems. However, the numerical studies on the simulation of behavior of Fe-SMA strengthened concrete elements as reported in literatures are even lesser.

In this paper, finite element (FE) modeling approach of concrete element with Fe-SMA strip has been presented. This method has been validated by comparing the computed results of the present study with that reported by Abouali et al. (2019). The validated modeling approach has been used as a tool to extend the understanding of effect of design variables such as concrete strength and Fe-SMA strip spacing on the constitutive behavior of concrete. Concrete Damage Plasticity (CDP) model available in ABAQUS has been used to model 15 numbers of 150 mm × 300 mm concrete cylinders with three different concrete strengths and four different SMA strip-spacing.

In this study, effect of Fe-SMA strip spacing and concrete grade on peak strength and ductility of the concrete cylinders is evaluated. It is observed that the residual stress of Fe-SMA confined concrete is independent of concrete strength and only a function of active confinement level for normal strength concrete. This establishes the effectiveness of Fe-SMA confinement in enhancement of strength and ductility of concrete.

*Keywords:* active confinement; Fe-SMA; finite element modeling; concrete damage plasticity.



## 1. Introduction

Plain concrete undergoes brittle failure when subjected to uniaxial compressive stress. Tests have shown that the addition of lateral confinement to concrete results in a significant increase in its strength and ductility. This is of utmost importance for structures to withstand extreme loads, such as earthquakes. Richart et al. [1] first studied the effectiveness of lateral confinement on the ductile failure of concrete. This research motivated several other researchers to come up with different methods to apply lateral confinement and assess the behavior of concrete under these confinement methods. There are mainly two types of concrete confinement: passive and active. In case of passive confinement, the confining pressure develops gradually after dilation of concrete during loading. Passive confinement techniques are widely used in the form of internal transverse reinforcement in new structures [2,3]. Mander et al. [3] proposed a stress-strain model for concrete under uniaxial compressive loading, confined by transverse reinforcements (spiral, circular hoops or rectangular hoops). For existing structures with insufficient ductility, passive confinement is commonly applied using external steel jackets and fiber-reinforced polymer (FRP) jackets. Many studies which focused on exploring the behavior of concrete confined by FRP jackets [4-8], modified the model proposed by Mander et al. [3] to predict the behavior of FRP confined concrete. Excellent corrosion resistance with high strength and stiffness to weight ratios makes FRP's one of the most suitable alternatives for concrete confinement as it does not alter the stiffness of the member which otherwise would impose additional seismic demand on it.

On the contrary, in case of active confinement, the lateral confining pressure is applied to concrete before the dilation of concrete. Previous studies [9-11] have demonstrated that under the same confinement pressure, active confinement approach by prestressed steel/FRP jackets is superior to passive confinement in terms of increasing the concrete strength and ultimate strain. A key factor behind such superiority is the delay in the damage sustained by the concrete as a result of the early application of confinement pressure in the case of active confinement; while in the case of passive confinement, the concrete would have to deform laterally in order for the confinement pressure to be fully activated. Methods of active confinement to repair damaged RC columns require a significant amount of time and labor along with specialized equipment. Hence, despite its advantages, its widespread application has been hindered, and the passive confinement approach using steel or FRP jackets has become more popular over the last several decades. Andrawes and Shin [12] first proposed the idea of using shape memory alloy (SMA) spirals to actively confine concrete through thermal prestressing, so as to improve its seismic performance. SMAs are a class of metallic alloys, which can undergo recovery of their original (undeformed) shape after being excessively deformed by heating the alloy to a temperature above the transformation temperature,  $A_f$ , which is a material property of the alloy predetermined by the user/manufacturer. This shape recovery is associated with the induction of large recovery stress in the SMAs when the prestrained alloy is heated while restrained. This recovery stress is utilized to exert active confinement pressure externally on concrete. Results indicated that this technique could be used for old as well as new structures. Later, several researchers [13-16] experimentally showed the enhancement of ultimate stress and ultimate strain of concrete confined by NiTiNb SMA spirals. Chen et al. [17] carried out FE analysis of concrete confined with NiTiNb spirals. More recently, Fe-based SMA systems are gaining popularity over NiTi-based SMAs due to low cost and ease of production. There are a very few experimental studies on the application of Fe-SMA in various civil engineering problems [18-20]. However, the numerical studies on the simulation of behavior of Fe-SMA strengthened concrete elements as reported in literature are even lesser. In this paper, FE modeling of concrete element with Fe-SMA strip has been presented and validated by comparing the computed results with that reported by Abouali et al. [21]. This validated modeling approach is then used to numerically predict and analyze the behavior of concrete confined by Fe-SMA strips using FE method.



## 2. FE modeling of concrete element with Fe-SMA strip

In the study, one reference beam and one beam strengthened with actively confined using near-surface mounted (NSM) Fe-SMA strips, from the experimental study carried out by Shahverdi et al. [18], were modeled. Load was monotonically applied to the beams in a four-point bending test. Details of modeling issues are discussed in the following sub-section.

### 2.1 Material Models

#### 2.1.1 Concrete constitutive model

To model the behavior of concrete, the CDP model available in ABAQUS was used [21]. In this model, damage is incorporated both in tension as well as compression. Concrete having cylindrical compressive strength,  $f_c'$  of 50 MPa and direct tensile strength,  $f_t$  of 2.4 MPa is used [18]. The stress-strain curve of concrete under uniaxial compression was defined using the Hognestad parabola, as described in Eq. (1) [22]:

$$\begin{aligned} \sigma_c^{(1)} &= E_{co} \varepsilon_c && \text{for } \sigma_c < 0.4 f_c' \\ \sigma_c^{(2)} &= f_c' \left[ 2 \left( \frac{\varepsilon_c}{\varepsilon_c'} \right) - \left( \frac{\varepsilon_c}{\varepsilon_c'} \right)^2 \right] && \text{for } \frac{\varepsilon_c}{\varepsilon_c'} \leq 1 \\ \sigma_c^{(3)} &= f_c' - \frac{f_c' (\varepsilon_c - \varepsilon_c')^2}{(\varepsilon_{c,max} - \varepsilon_c')^2} && \text{for } \frac{\varepsilon_c}{\varepsilon_c'} > 1 \end{aligned} \quad (1)$$

where,  $\sigma_c$  and  $\varepsilon_c$  are the compressive stress and strain respectively,  $\varepsilon_{c,max}$  is the maximum strain,  $\varepsilon_c'$  is the strain corresponding to the peak stress,  $E_{co}$  is the modulus of elasticity of concrete. The resulting stress-strain curve is shown in Fig.1 (a). In tension, the stress-crack opening displacement curve post-cracking of concrete was defined in the ABAQUS CDP model by an exponential function described by Eq. (2) [23]:

$$\begin{aligned} \frac{\sigma}{f_t} &= f(w) - \frac{w}{w_c} f(w_c) \\ \text{where, } f(w) &= \left[ 1 + \left( \frac{c_1 w}{w_c} \right)^3 \right] \exp\left( -\frac{c_2 w}{w_c} \right) \text{ and } w_c = 5.14 \frac{G_f}{f_t} \end{aligned} \quad (2)$$

where,  $w$  is the crack opening displacement,  $w_c$  is the crack opening displacement at which no stresses can't be transferred,  $f(w)$  is a displacement function,  $G_f$  is the concrete fracture energy, and  $c_1$  and  $c_2$  are material constants. The resulting graph is shown in Fig.1 (b).

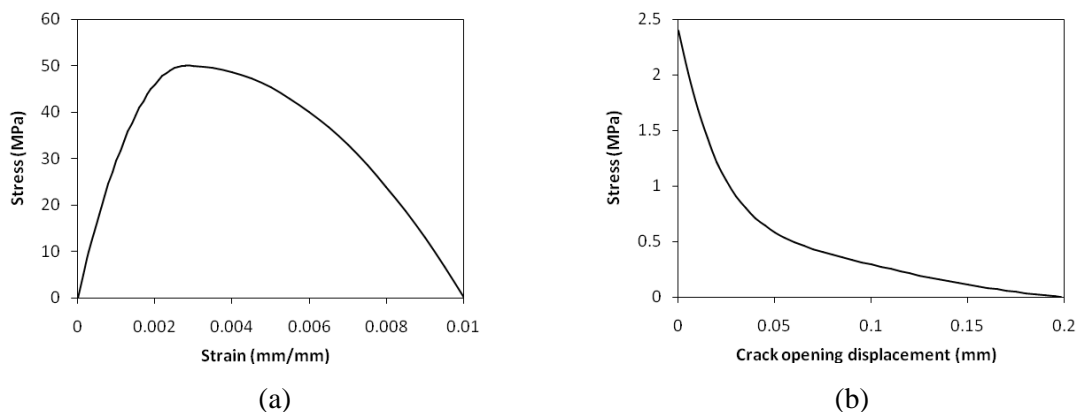


Fig. 1 – Stress-strain curve of concrete under: (a) compression (b) tension [21]



The values of the plasticity parameters used in this study are summarized in Table 1. Compressive and tensile damage variables in the CDP model are defined as per [24].

Table 1 – Plasticity parameters for CDP model [21]

Dilation angle, $\Psi$ ( $^{\circ}$ )	50
Plastic potential eccentricity, $\varepsilon$	0.1
Stress ratio, $\sigma_{b0}/\sigma_{c0}$	1.16
Shape of the yielding surface, $K_c$	0.667
Viscosity parameter, $\mu$	0.0001

### 2.1.2 Steel reinforcement and iron-based shape memory alloy (Fe-SMA) strips

To model the longitudinal and transverse steel reinforcements, an isotropic hardening plasticity model was used. A trilinear elasto-plastic stress-strain curve [21] as shown in Fig. 2 (a) was incorporated. The elastic modulus and yield stress of the steel were taken as 205 GPa and 508 MPa, respectively.

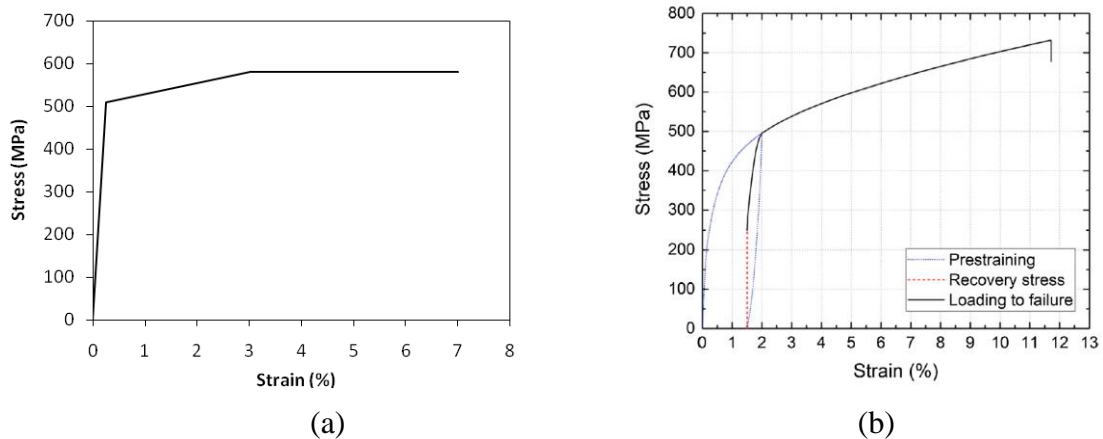


Fig. 2 – Stress-strain curve for: (a) steel reinforcement (b) activated Fe-SMA [21]

The Fe-SMA strips were modeled with the stress-strain curve obtained in the tension test [18], using isotropic hardening plasticity as shown in Fig. 2(b). For the beam with activated Fe-SMAs, the loading to failure segment of the stress-strain diagram was implemented in the FE model. As debonding failure was not observed at the interface in the tested beams, a tie constraint was considered at the concrete-grout interface.

### 2.1.3 Grout

Compressive strength, tensile strength, and elastic modulus of the grout were considered as 90 MPa, 3.2 MPa, and 37.2 GPa, respectively as per Shahverdi et al. [18]. A CDP model was used to model the behavior of the grout.

### 2.2 FE model of sample beams

The dimensions and cross-sectional details of the beams are shown in Fig. 3 (a). Due to mid-span and mid-section symmetry only one quarter of the beams was modeled.

Continuum eight-node linear brick elements with reduced integration and hourglass control (C3D8R) were used to model the concrete and grout. The reinforcement was modeled by two-node linear truss



elements (T3D2) and the Fe-SMA strips were modeled with two-node Timoshenko beam elements (B31) with linear interpolation.

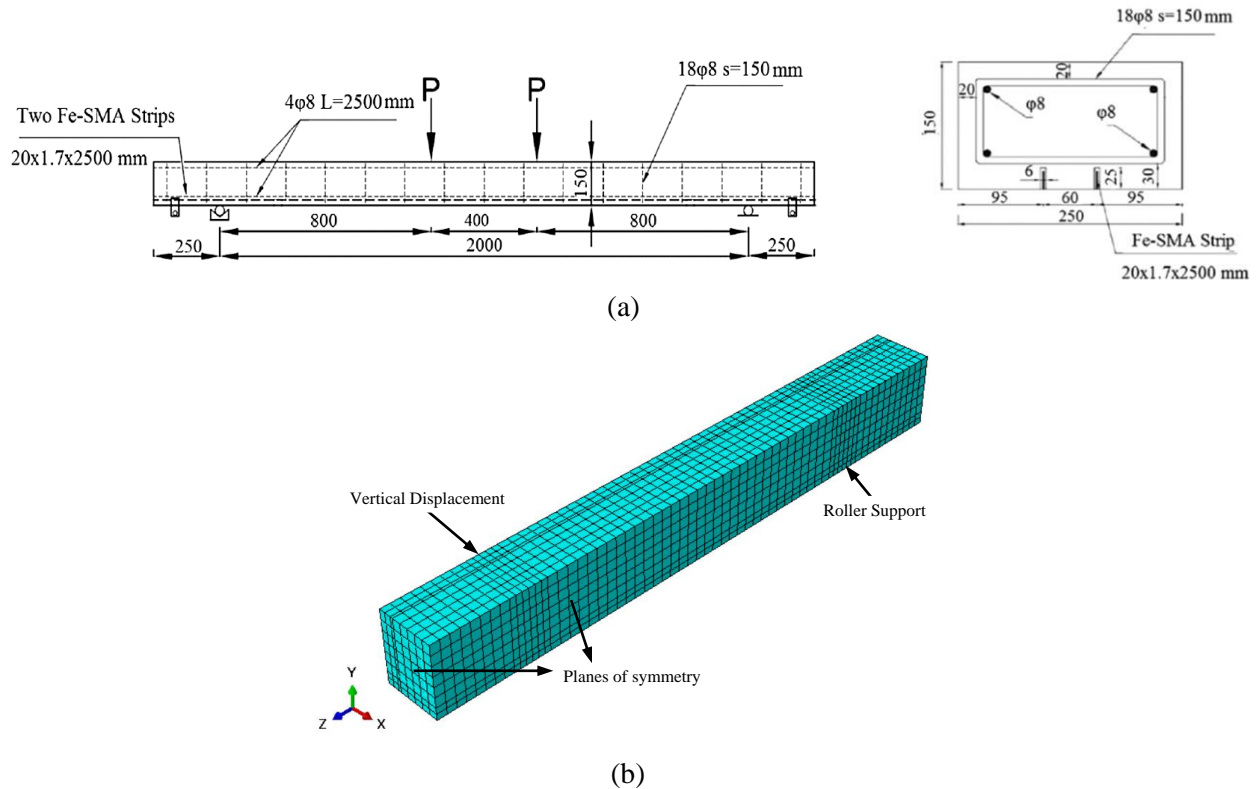


Fig. 3 – Fe-SMA strengthened beams (a) dimensions and cross-sectional view [18] (b) mesh configuration

For mid-span and mid-section planes of symmetry in the beam, ‘Symmetry’ boundary conditions were used. The “Embedded Region” constraint was used for embedding the longitudinal and transverse reinforcements in the concrete as well as embedding the Fe-SMA elements in the grout. This is because, during experiments, relative slips were not observed between the Fe-SMA strips and grout.

Using the initial stress feature in ABAQUS, the recovery stress was enforced as initial stress in the Fe-SMA strips in the axial direction. To allow establishment of self-equilibrium after assigning the initial stress, an idle step without any loading was defined.

Displacement-controlled loading was applied to the models by applying a monotonic vertical displacement with a loading strain rate of 0.5% per m until failure of the beam [18]. The nonlinear solution was then obtained by configuring an implicit static general analysis method.

### 2.3 Results and discussion

Load vs. mid-span deflection curves for the reference beam and that for the beam with Fe-SMA strips, as NSM reinforcement, obtained from the FE simulations are compared with those obtained from Abouali et al. [21] in Figs. 4 (a) & (b). Beam with Fe-SMA shows a 60% increase in the load carrying capacity as compared to the control beam. Results obtained are in close agreement with the results from Abouali et al. [21] which demonstrates the good predictive performance of the adopted numerical model.

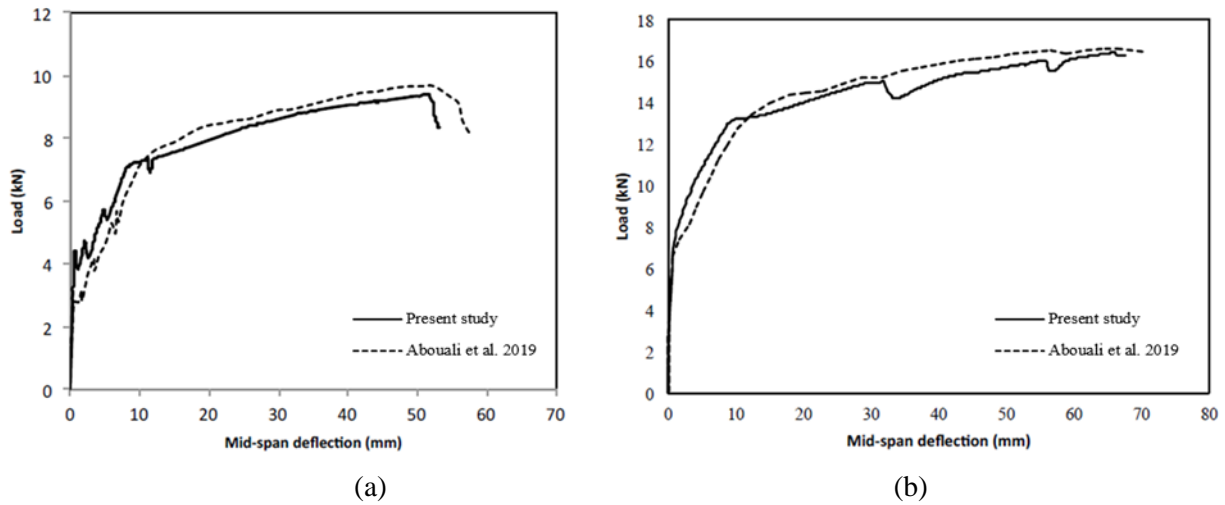


Fig. 4 – Comparison of FE simulated load-deflection curves of present study and those reported by Abouali et al. [21] for: (a) control beam (b) beam with Fe-SMA as NSM reinforcement

### 3. Parametric study on concrete confined with Fe-SMA strips

The FE modeling approach presented in the previous section can be used as a practical and cost-effective tool to perform parametric numerical studies on the effect of design variables. To understand how concrete grade and Fe-SMA strip spacing affect the constitutive behavior of concrete, standard concrete cylinders of 150 mm diameter and 300 mm height were modeled for FE simulation. Three different concrete grades of characteristic strength 25 MPa, 30 MPa and 40 MPa, which are designated as A, B and C respectively, are considered in this study.

To understand the effect of Fe-SMA strip spacing on the constitutive behavior of concrete, four different SMA strip spacing are adopted in the study. The dimensions of Fe-SMA strips used are: 24 mm width and 1.5 mm thickness. Four different strip spacing of 92 mm, 69 mm, 55.2 mm and 46 mm, which are designated as S1, S2, S3 and S4, are considered in this parametric study. Hence specimen A-S1 implies M25 grade concrete cylinder with Fe-SMA spacing of 92 mm.

Previous studies on active confinement have shown that the axial stress-strain response of concrete under monotonic loading appears to be the envelope of axial stress-strain response of cyclically loaded concrete [16]. Hence in this study, the cylinders were subjected to monotonic loading only.

Active confining pressures corresponding to different strip spacing were calculated based on the effective confining pressure proposed by Mander et al. [3]. According to Mander et al. [3], for a circular section, the effective confining pressure  $f_l'$  can be calculated as:

$$f_l' = \frac{2k_e f_h A_{sp}}{sD} \quad (3)$$

where,  $k_e$  is the confinement effectiveness ratio,  $f_h$  is the SMA recovery stress [16],  $A_{sp}$  and  $s$  are the cross-sectional area and centre-to-centre spacing of the Fe-SMA strip and  $D$  is the diameter of the specimen.

#### 3.1 Finite element model

Continuum eight-node linear brick elements with reduced integration and hourglass control (C3D8R) were used to model the concrete as it provides a solution of comparable accuracy as compared to second order tetrahedral elements at less computational cost. Fe-SMA strips, as shown in Fig. 5, were modeled with two-node Timoshenko beam elements (B31) with linear interpolation as it can be subjected to large axial strains.



Material model of concrete and Fe-SMA was adopted from the previously validated numerical model. Assuming no slip between the SMA strips and concrete surface, a “tie” constraint was used to model the interaction between the two. A fixed boundary condition was applied to the bottom surface of the model during loading phase. Modeling of prestressing and loading conditions was kept same as that described in the previous section.

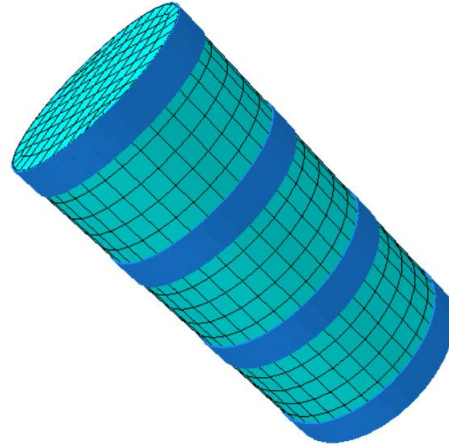


Fig. 5 – FE model of concrete cylinder confined by Fe-SMA strips

### 3.2 Results and discussion

A parametric study is carried out to understand the effect of concrete strength and Fe-SMA strip spacing on the constitutive behavior of concrete. The results of all the specimens are summarized in Table 2.

Table 2 – Summary of results for all specimens

Specimen	Active confinement pressure (MPa)	$f_{cc}'$ (MPa)	$f_{res}$ (MPa)
A	0	19.6	-
A-S1	1.09	29.7	15.2
A-S2	1.76	33.9	21.9
A-S3	2.44	35.6	26.8
A-S4	3.14	45.2	32.7
B	0	23.5	-
B-S1	1.09	34.1	15.4
B-S2	1.76	38.3	22.1
B-S3	2.44	40.8	26.9
B-S4	3.14	49.5	32.8
C	0	30.9	-
C-S1	1.09	42.9	15.1
C-S2	1.76	47.1	22.1
C-S3	2.44	49.2	27.1
C-S4	3.14	58.1	32.9



### 3.2.1 Effect of grade of concrete

Four spacing values were considered in the study namely 92 mm, 69 mm, 55.2 mm and 46 mm. Fig. 6 compares the axial stress-strain relationships of SMA confined concrete having same strip spacing with different concrete grades.

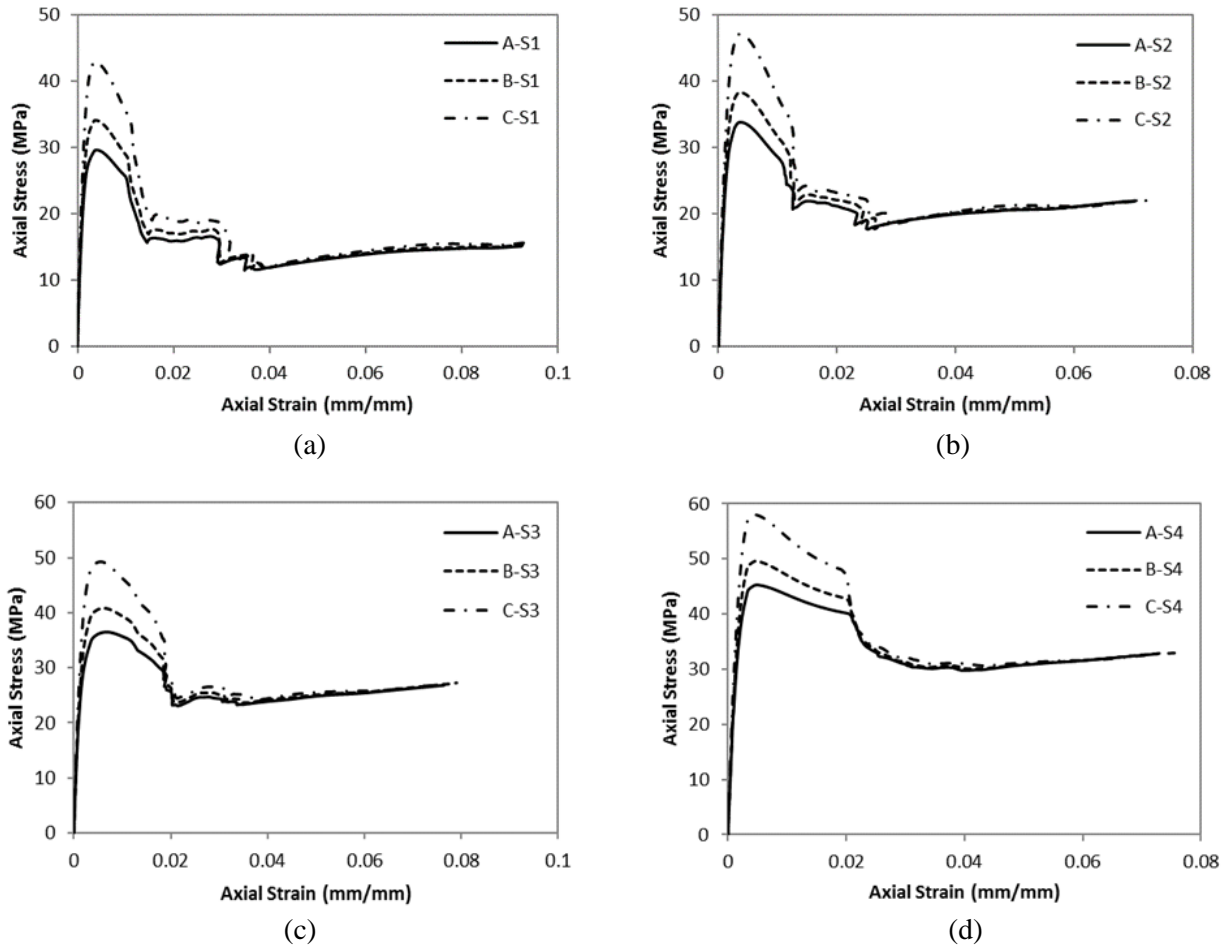


Fig. 6 – Comparison of axial stress-strain relationships of Fe-SMA confined concrete of different grades (A= 25 MPa, B= 30 MPa & C= 40 MPa) for strip spacing: (a) 92 mm (b) 69 mm (c) 55.2 mm (d) 46 mm

As the grade of concrete is increased from M25 to M40, it is observed that the peak stresses of A-S1, B-S1, C-S1 increased by 51%, 45.3% and 38.9% respectively as compared to that of their respective unconfined concrete specimens A, B and C. However, residual stress of Fe-SMA confined concrete is found to be independent of concrete grade and is only a function of active confinement level for normal strength concrete. Similar trend is observed for specimens with SMA spacing of S2, S3 and S4. This observation is in agreement with the experimental results obtained by Chen et al. [16] for NiTiNb-SMA spirals confined concrete.

### 3.2.2 Effect of spacing of Fe-SMA strips

As the spacing of Fe-SMA strips is decreased from S1 to S4, the effective confinement pressure exerted by the strips on concrete increases. With increasing value of confinement pressure, it is observed (Fig. 7) that the peak stresses of A-S1 to A-S4 increased by 51%, 72.9%, 81.6% and 130% respectively as compared to that of the unconfined concrete specimen, A. From Fig. 7, it is evident that the ductility of the specimens also increases as compared to that of the unconfined specimen. Also, as established in the earlier section, residual



stress is a function of confinement level of concrete. Thus, with increase in the confinement value of Fe-SMA strips the residual stress increases. Similar trend is observed for specimens of grade of concrete B, C when the spacing is varied from S2 to S4.

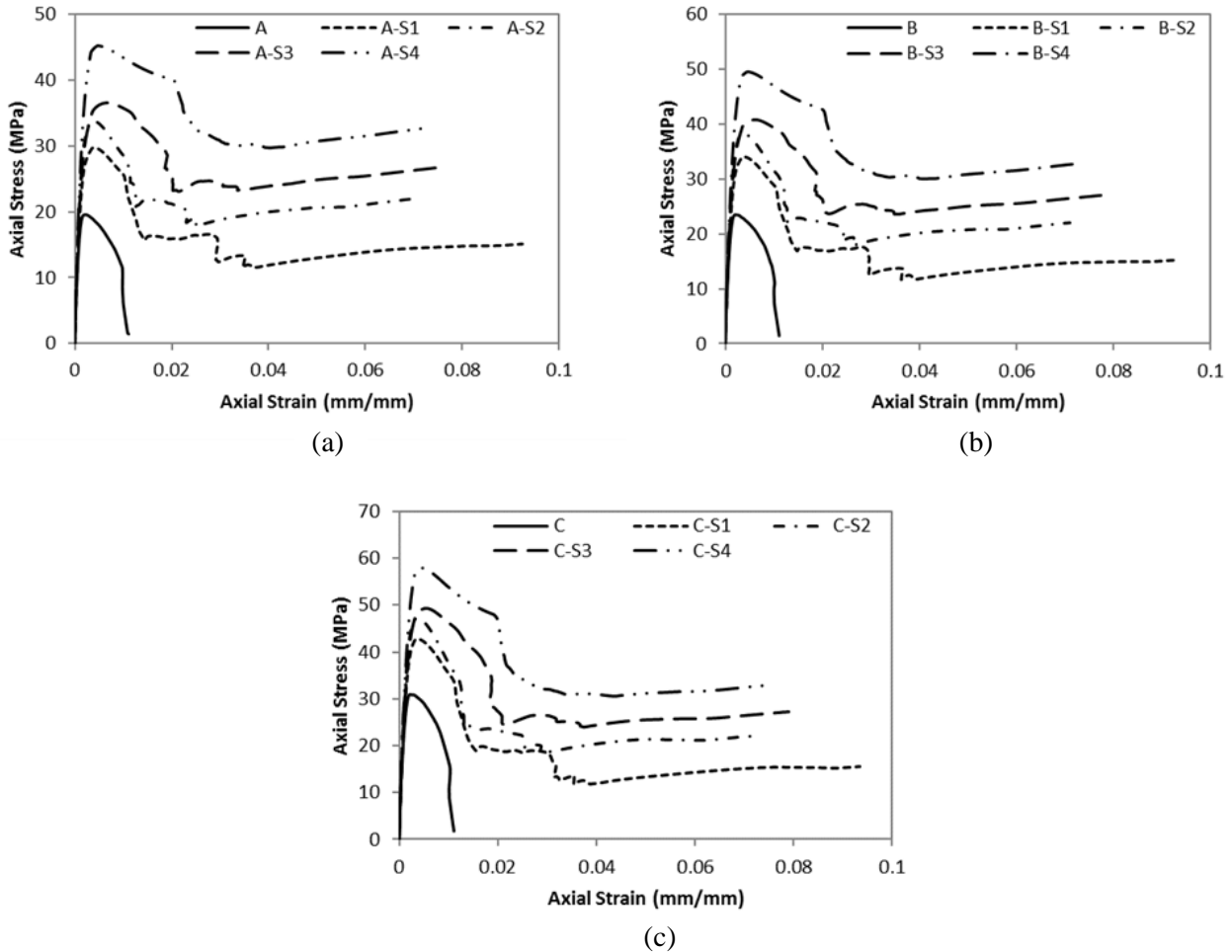


Fig. 7 – Comparison of axial stress-strain relationships of Fe-SMA confined concrete having different strip spacing (S1= 92mm, S2= 69mm, S3= 55.2mm & S4= 46 mm) for concrete grades (a) 25 MPa (b) 30 MPa (c) 40 MPa

#### 4. Conclusion

This study focused on analyzing the behavior of SMA confined concrete using FEM within the framework of damaged plasticity model in ABAQUS. Active confinement of concrete is provided by prestrained SMAs which are restrained while heating. This is due to induction of large recovery stresses in the SMA, as it tries to recover its original undeformed configuration. This study is an initial step towards understanding the behavior of Fe-SMA confined concrete by numerically investigating the change in the constitutive behavior of concrete with changes in grade of concrete and SMA spacing. Concrete cylinders, 150 mm diameter and 300 mm height, having three different concrete grades of 25 MPa, 30 MPa and 40 MPa and four different SMA strip-spacing of 92 mm, 69 mm, 55.2 mm and 46 mm were modeled and simulated under uniaxial compressive monotonic loading. The results show that there is an increase in the strength as well as ductility of the concrete specimens due to this active confinement.



The following conclusions could be drawn from the study:

1. The effectiveness of Fe-SMA confinement on concrete strength and ductility enhancement increases as the active confinement pressure increases.
2. The residual stress of Fe-SMA confined concrete is independent of concrete strength and only function of active confinement pressure on concrete.
3. Therefore, it may be concluded that active confinement would provide enhanced seismic performance by increasing both strength and ductility of concrete.

## 5. References

- [1] Richart FE, Brandtzaeg A, Brown RL (1928): A study of the failure of concrete under combined compressive stresses. University of Illinois at Urbana Champaign, College of Engineering, Engineering Experiment Station.
- [2] Sheikh SA, Uzumeri SM (1982): Analytical model for concrete confinement in tied columns. *Journal of the Structural Division*, **108** (12), 2703-22.
- [3] Mander JB, Priestley MJ, Park R (1988): Theoretical stress-strain model for confined concrete. *Journal of structural engineering*, **114** (8), 1804-26.
- [4] Mirmiran A, and Shahawy M (1995): A novel FRP-concrete composite construction for the infrastructure. *Proceedings of Structures Congress XIII*, 1663-1666.
- [5] Jiang T, Teng JG (2007): Analysis-oriented stress-strain models for FRP-confined concrete. *Engineering Structures*, **29** (11), 2968-86.
- [6] Yu T, Teng JG, Wong YL, Dong SL (2010a): Finite element modeling of confined concrete-I: Drucker-Prager type plasticity model. *Engineering Structures*, **32** (3), 665-79.
- [7] Yu T, Teng JG, Wong YL, Dong SL (2010b): Finite element modeling of confined concrete-II: Plastic-damage model. *Engineering structures*, **32** (3), 680-91.
- [8] Teng J, Huang YL, Lam L, Ye LP (2007): Theoretical model for fiber-reinforced polymer-confined concrete. *Journal of composites for construction*, **11** (2), 201-10.
- [9] Miyagi T, Yamakawa T, Li W, Rahman M (2004): A study of emergency retrofit using prestressing bars and steel plates for damaged columns. *Proceedings of Thirteenth World Conference on Earthquake Engineering*, Vancouver, Canada.
- [10] Nesheli KN, Meguro K (2006): Seismic retrofitting of earthquake-damaged concrete columns by lateral pre-tensioning of FRP belts. *Proceedings of 8th US National Conference on Earthquake Engineering*, San Francisco, U.S.
- [11] Moghaddam H, Samadi M, Pilakoutas K, Mohebbsi S (2010): Axial compressive behavior of concrete actively confined by metal strips; part A: experimental study. *Materials and Structures*, **43**(10),1369-81.
- [12] Andrawes B, Shin M (2008): Seismic retrofitting of bridge columns using shape memory alloys. *Active and Passive Smart Structures and Integrated Systems*, **6928**: 69281K, International Society for Optics and Photonics.
- [13] Shin M, Andrawes B (2010): Lateral cyclic behavior of reinforced concrete columns retrofitted with shape memory spirals and FRP wraps. *Journal of Structural Engineering*, **137** (11), 1282-90.
- [14] Choi E, Chung YS, Kim YW, Kim JW (2011): Monotonic and cyclic bond behavior of confined concrete using NiTiNb SMA wires. *Smart Materials and Structures*, **20** (7), 075016.
- [15] Dommer K, Andrawes B (2012): Thermomechanical characterization of NiTiNb shape memory alloy for concrete active confinement applications. *Journal of Materials in Civil Engineering*, **24** (10), 1274-82.
- [16] Chen Q, Andrawes B (2017): Cyclic stress-strain behavior of concrete confined with NiTiNb-shape memory alloy spirals. *Journal of Structural Engineering*, **143** (5), 04017008.
- [17] Chen Q, Andrawes B (2014): Finite element analysis of actively confined concrete using shape memory alloys. *Journal of Advanced Concrete Technology*, **12**(12), 520-34.



- [18] Shahverdi M, Czaderski C, Motavalli M (2016): Iron-based shape memory alloys for prestressed near-surface mounted strengthening of reinforced concrete beams. *Construction and Building Materials*, **112**, 28-38.
- [19] Pan S, Hu M, Zhang X, Hui H, Wang S (2018): A new near-surface-mounted anchorage system of shape memory alloys for local strengthening. *Smart Materials and Structures*, **28**, 025016.
- [20] Hong K, Lee S, Yeon Y, Jung K (2018): Flexural Response of Reinforced Concrete Beams Strengthened with Near-Surface-Mounted Fe-Based Shape-Memory Alloy Strips. *International Journal of Concrete Structures and Materials*, **12** (1), 45.
- [21] Abouali S, Shahverdi M, Ghassemieh M, Motavalli M (2019): Nonlinear simulation of reinforced concrete beams retrofitted by near-surface mounted iron-based shape memory alloys. *Engineering Structures*, **187**, 133-48.
- [22] Hognestad E (1951). Study of combined bending and axial load in reinforced concrete members. University of Illinois at Urbana Champaign, College of Engineering. Engineering Experiment Station.
- [23] Cornelissen H, Hordijk D, Reinhardt H (1986): Experimental determination of crack softening characteristics of normalweight and lightweight. *Heron*, **31** (2), 45-56.
- [24] Birtel V, Mark P (2006): Parameterised finite element modelling of RC beam shear failure. *ABAQUS users' conference*, 95-108.